IOP Publishing Plasma Physics and Controlled Fusion
Plasma Phys. Control. Fusion **62** (2020) 035004 (9pp) https://doi.org/10.1088/1361-6587/ab630f

Radio frequency emissions driven by energetic ions from neutral beam in KSTAR low confinement mode plasma

Shekar G Thatipamula[1], M H Kim[1,2], J Kim[2], J H Kim[2] and G S Yun[1]

[1] Pohang University of Science and Technology, Pohang, Gyeongbuk 37673, Republic of Korea
[2] National Fusion Research Institute, Daejeon 34133, Republic of Korea

E-mail: gunsu@postech.ac.kr

Received 21 October 2019, revised 29 November 2019
Accepted for publication 17 December 2019
Published 16 January 2020

Abstract

The tangential neutral beam injection in KSTAR low confinement mode plasma is rapidly accompanied by the electromagnetic emissions in radio frequency (RF) range (0.1–1 GHz). The RF emission is initially onset within 1 ms from the beam injection, at discrete frequencies with steadily increasing intensity. The frequency spacing for these discrete emission lines corresponds to the deuteron cyclotron frequency, at a location midway between the magnetic axis and the edge. Further, the observed discrete frequencies lie in the lower hybrid frequency (f_{LH}) range in a broad region on the low field side (LFS). As the initial RF emission becomes saturated, there is another onset of intense RF bursts occurring at discrete frequencies, broadening the emission frequency range further, either at higher or lower frequencies. In some cases, the time interval of the intense RF bursts at the dominant frequency is comparable with the toroidal rotation period at the radial location where $f_{LH} \sim$ dominant frequency. The rapid rise and saturation of RF emission intensity in a broad frequency range indicate that a small population of fast ions is sufficient for the growth of energetic particle driven instabilities on the LFS. The multiple onsets in RF emission and the intense RF burst repetition frequency comparable with toroidal rotation frequency indicate the possibility that reorganization in the anisotropic fast ion population results in localized growth of the above instabilities. A gradual decay of RF emission intensity over few tens of milliseconds indicate that enhanced population of fast ions has damping effect on these instabilities.

Keywords: radio frequency burst, lower hybrid frequency, ion cyclotron emission, neutral beam injection, KSTAR tokamak, RF spectrometer

(Some figures may appear in colour only in the online journal)

1. Introduction

Investigation of the energetic particle confinement and interaction with the turbulence have gained momentum in recent decades as the fusion research community is preparing for reactor level research [1]. The energetic particles can result from the fusion reactions or the auxiliary heating systems. It is widely believed that confinement of the energetic particles holds the key for self-sustenance of the fusion reactions [2]. A range of Alfvén eigenmodes and other magnetohydrodynamic modes driven by the energetic particles is evident from the observations on fusion devices [3–5]. Their localization, growth and damping mechanisms are investigated currently in the pursuit for a sustainable reactor [6].

In the previous works, detection of electromagnetic bursts in the radio frequency (RF) range, using the RF spectrometer from the KSTAR plasma at the edge-localized mode (ELM) crashes was reported [7]. The RF emission evolves in multiple steps from a narrowband frequency prior to the ELM crash to a wideband frequency range at the crash [8]. Further, the emergence of a non-modal filamentary perturbation and its burst onset in the plasma edge coincide with

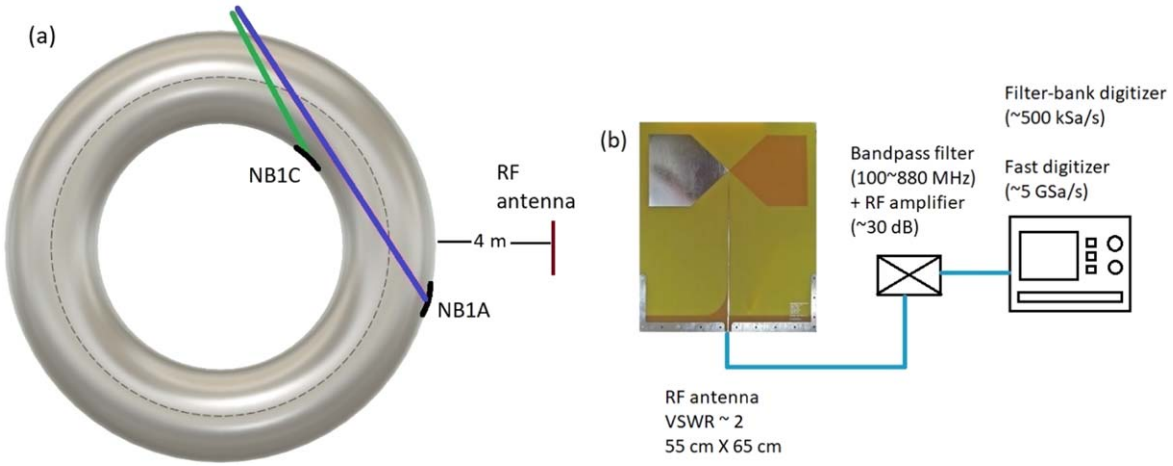

Figure 1. (a) Schematic top view of the neutral beam injection and RF antenna on KSTAR tokamak. The major and minor radii are 1.8 m and 0.5 m respectively. The black arcs indicate shine-through armors at in-vessel boundary. NB1C has the least tangential radius. The colours depicting the neutral beam path are chosen consistently with the time traces of neutral beam power in the following figures. (b) The RF spectrometer system is shown schematically with the antenna, the transmission line and the digitizer. The digitizer symbolically represents the data acquisition using filter-bank spectrometer digitizers at 0.5 MSa s^{-1} and a fast digitizer at 5 GSa s^{-1}.

the intensifying of the discrete spectral lines and the onset of wideband emission respectively [9]. A rapid chirping in steps of ion cyclotron harmonics at the onset of pedestal collapse was understood to be due to rapid evolution in density in the plasma edge [10, 11].

Observation of the RF emission at harmonics of the deuteron cyclotron frequency in the edge, persistently occurring in the inter-ELM crash period and intensifying prior to the crash [8, 9], has motivated deeper investigation in to the role of fast ions from the neutral beams. In this paper, novel observations on the RF emission using the RF spectrometer, with the neutral beam injection (NBI) in the KSTAR low confinement (L-)mode plasma are reported. A brief description of the RF spectrometer, typical features in the RF emission and spectrum is given in section 2. A shift in the RF emission frequency range on varying the electron density and relevance to characteristic frequencies is described in section 3. Evolution of the fully resolved spectrum with the start of beam injection is described in section 4. In section 5, important factors possibly affecting the RF emission and spectrum are described. Plausible mechanisms based on the observed spectral features and spatio-temporal evolution are mentioned in section 6.

2. RF emissions with NBI in L-mode discharges

Electromagnetic emissions in the frequency range 0.1–1 GHz from KSTAR plasma are detected using the RF spectrometer. KSTAR is a medium size tokamak with major and minor radii of 1.8 m and 0.5 m respectively. The neutral beam system on KSTAR consists of three beamlines with a combined maximum heating power of 5 MW until 2017 experiments [12]. A schematic injection of the two neutral beamlines on KSTAR from top view, used for the results described in this article, is shown in figure 1(a). The RF spectrometer system on KSTAR and measurement schemes were thoroughly described in references [7–9] and shown schematically in figure 1(b). The RF spectrometer consists of a bow-tie or a spiral antenna 4 m away from the plasma edge, facing the fused silica vacuum viewport outside the vacuum vessel, a transmission line and digitizers. A two-module RF filter-bank with 8 channels each, spanning a total frequency range of 40–800 MHz acquires the RF burst signals typically at 500 kSa s^{-1}, often for the entire duration of the discharge. The bandwidths of RF filters whose results are included in this article are approximately ±25% of their center frequency. In addition, the RF burst signals are also acquired by a fast digitizer at 5 GSa s^{-1} for a total duration of 100 ms or less. Due to the limit in total acquisition time, the fast digitizer is triggered at specific intervals of interest during the KSTAR discharges.

RF bursts are detected with the injection of neutral beam in several L-mode discharges in KSTAR. The time traces of filter-bank RF spectrometer signals along with the neutral beam power for KSTAR shot 16 485 are shown in figure 2(a). A brief summary of the discharge conditions is as follows. The toroidal magnetic field at the magnetic axis (B_0) = 2.5 T and the toroidal plasma current (I_p) is ~0.5 MA. The neutral beam is applied in pulses of 20 ms duration at 2 Hz frequency using only one beam of energy 100 keV with heating power (P_{NB}) = 1.6 MW. The line averaged electron density ($\langle n_{e,\,int}\rangle$) is $\sim 0.8 \times 10^{19}$ m^{-3} initially (at 2.77 s). The text labels in MHz on the panels for filter-bank RF channels indicate the center frequencies for corresponding RF filters, whose output voltage represents the emission intensity. The RF emission intensity increases within 0.5 ms of the beam injection which is comparable to the sampling interval of the neutral beam power. Hence there is no significant delay in the onset of RF emission with respect to the beam injection within this sampling time resolution. As the RF emission intensity becomes saturated, there is onset of intense RF bursts with a delay of 1.5–2 ms with respect to the initial onset of RF emission. The intense RF bursts are initially confined to a lower frequency range (around 400 MHz), later spreading to further lower

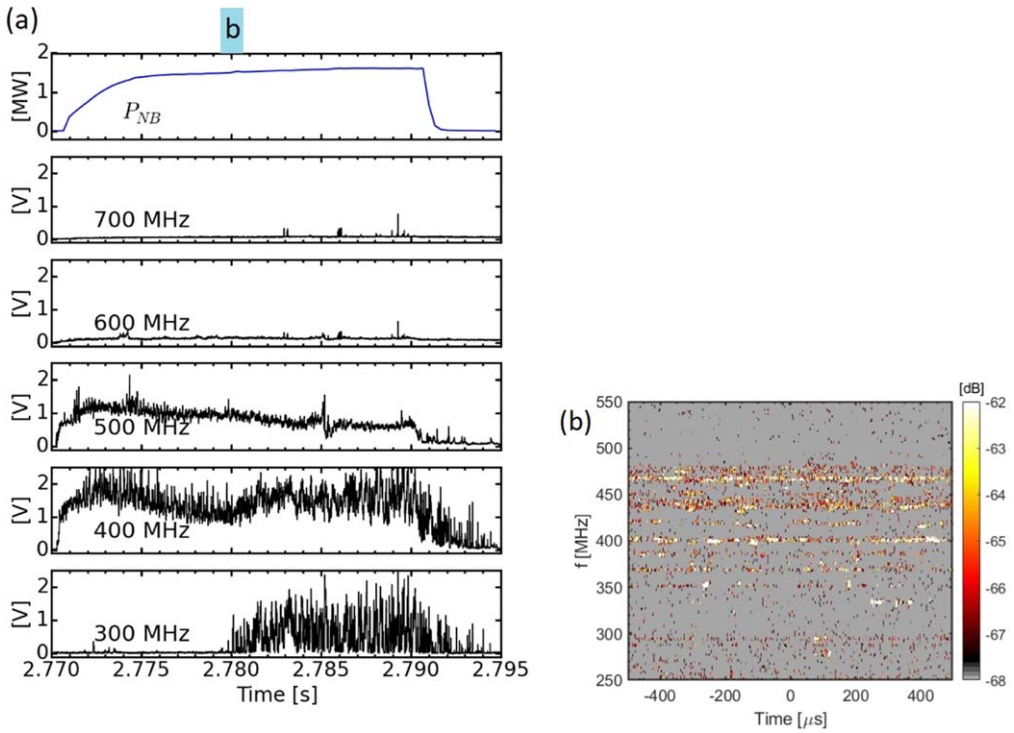

Figure 2. RF spectrometer signals with neutral beam pulse for shot 16 485. Shot parameters: $B_0 = 2.5$ T, $I_p \sim 0.5$ MA and the line averaged density ($\langle n_{e,\,\mathrm{int}} \rangle$) is initially (at 2.77 s) $\sim 0.8 \times 10^{19}$ m^{-3}. (a) Top panel shows the neutral beam power and other panels depict filter-bank RF intensity in units of 'volts' with text labels in the figure panels indicating the center frequencies of RF filters. (b) The spectral evolution of RF emission acquired on fast digitizer for 1 ms time window illustrated with cyan block labeled 'b' on top panel of figure 2(a). The center of the segment (time = 0) corresponds to 2.780 000 s from the plasma startup.

frequencies (300–400 MHz) with a delay of 10 ms in this case. On the other hand, the RF emission intensity in 500 MHz range continues to decrease gradually until the neutral beam is turned off.

The fully resolved RF emission spectrum is obtained through the fast digitizer acquisition for 1 ms long segments in the above KSTAR discharge. The fast digitizer was triggered at regular intervals of 20 ms, capturing RF emission for 1 ms at 5 GSa s^{-1} on each trigger. The fast digitizer time trace is split into bins of 4096 data points for plotting the RF spectral evolution, resulting in 1.2 MHz frequency resolution. Figure 2(a) is an example of RF emission occurring at a neutral beam pulse described above and figure 2(b) shows its spectral evolution for a data segment captured during the beam pulse. The horizontal center of the segment 'zero' corresponds to the trigger instant (2.780 000 s with respect to the plasma startup) and is approximately in the middle of the neutral beam pulse marked in figure 2(a). The fully resolved RF emission spectrum in figure 2(b) depicts that the RF emission occurs at discrete frequencies. In the upper frequency range, an emission line occurs persistently at 470 ± 1.2 MHz. In the lower frequency range, the RF emission occurs mostly as bursts, often with uniformly spaced lines between 340–420 ± 1.2 MHz. The frequency spacing is 17 MHz which corresponds to the deuteron cyclotron frequency at $R \sim 2.0$ m and hence the discrete spectral lines in the lower frequency range correspond to the deuteron cyclotron harmonics.

3. Shift in RF emission frequency range with electron density variation

The gradual increase in the line averaged density in the above KSTAR discharge (shot 16 485) resulted in a remarkable evolution in the RF emission spectrum observed through the filter-bank RF spectrometer. The filter-bank RF intensity is shown in figure 3(a) along with $\langle n_{e,\,\mathrm{int}} \rangle$ and the neutral beam power. The radial profile of local electron density (n_e) obtained from Thomson scattering diagnostic is compared for 2.767 and 5.767 s in figure 3(b). As $\langle n_{e,\,\mathrm{int}} \rangle$ increases from 0.8 to 1.8 $\times$ 10^{19} m^{-3}, the saturated RF emission frequency range shifts gradually to higher frequencies, that is from 300–500 MHz to 500–700 MHz for neutral beam pulses at 2.77 s and 5.77 s respectively. The fully resolved RF emission spectrum shown in figure 2(b) corresponding to 2.780 000 s illustrates the actual RF emission frequency range as 340–470 MHz ± 1.2 MHz, consistent with the observations through filter-bank RF spectrometer. Assuming the local electron density varies linearly for 1.85 m $< R <$ 2.1 m and considering the local magnetic field, the lower hybrid frequency is estimated as follows. The lower hybrid frequency is given by

$$f_{LH} = \frac{1}{2\pi}\left(\frac{1}{\Omega_e \Omega_i} + \frac{1}{\omega_{pi}^2}\right)^{-1/2},$$

where $\Omega_e = eB/m_e$ and $\Omega_i = eZB/m_i$ indicate the angular cyclotron frequencies of electron and ion respectively, with

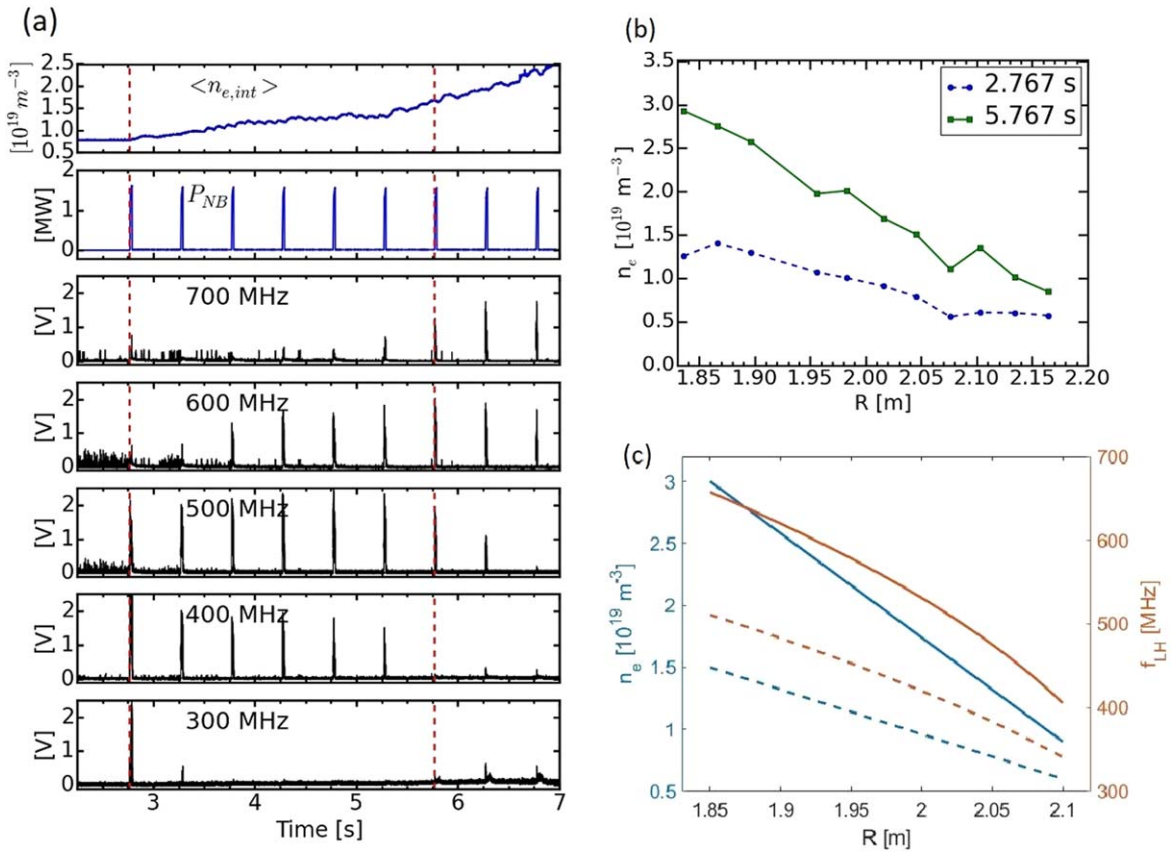

Figure 3. Evolution of the RF emission spectrum with n_e variation for shot 16 485 and comparison with characteristic local frequencies. The emission spectrum shifts upward in frequency with increasing density. (a) The time traces of filter-bank RF spectrometer channels in units of volts along with the neutral beam power and line averaged electron density ($\langle n_{e,\,\mathrm{int}}\rangle$) from microwave interferometer. (b) Comparison of the electron density profiles from Thomson Scattering diagnostic prior to the NBI at the instants marked by red dashed lines in figure 3(a). (c) f_{LH} estimated using n_e values at 1.85, 2.1 m and assuming linear variation between them from Thomson Scattering data for low and high n_e shown in figure 3(b). Blue lines indicate the approximated n_e and orange curves indicate the corresponding f_{LH}. Low density case is shown in dashed line and curve and the high density case is shown in solid line and curve. The fully resolved RF emission frequency range in figure 2(b), corresponds to f_{LH} in a very broad region on the LFS (1.9–2.1 m) illustrated in orange dashed curve. At high n_e, the RF emission frequency range (at the second red dashed line in figure 3(a)) is consistent with the f_{LH} illustrated in orange solid curve. The major and minor radii are 1.8 m and 0.5 m respectively.

e, m_e, m_i and B indicating the magnitude of electron charge, electron mass, deuterium ion mass and the local magnetic field respectively and $Z = 1$ is the charge state of deuteron; $\omega_{pi} = \sqrt{n_i Z^2 e^2/m_i \epsilon_0}$ indicates the ion plasma frequency with n_i ($\approx n_e$) is the ion density and ϵ_0 is the free space permittivity. From Thomson scattering diagnostic measurements n_e varies between 1.5–0.6 $\times$ 10^{19} m^{-3} for 1.85 m $< R <$ 2.1 m at 2.767 s; at 5.767 s n_e varies between 3.0–0.9 $\times$ 10^{19} m^{-3} in the same radial range. The assumed local density profiles at 2.767 s and 5.767 s are shown in dashed and solid lines respectively on the left vertical axis (blue) in figure 3(c). The curves on the right vertical axis (orange) in figure 3(c) indicate the corresponding f_{LH}. Comparing the spectral frequency range in figure 2(b) and dashed orange curve in figure 3(c) suggests that the RF emission spectrum corresponds to the f_{LH} in a broad region on the LFS (1.9–2.1 m).

The above observations indicate that RF emission occurs due to the excitation of waves by energetic ions from the neutral beam. The observed frequency spectrum of RF emission suggests that the wave excitation primarily occurs through instabilities in LH frequency range. The upward shift in the frequency range of RF emission with increasing electron density confirms further the density dependency and hence the LH range instabilities as responsible for the RF emission.

4. Evolution of the RF emission on the NBI

As the multiple spikes in figure 2(a) suggest that the RF emission occurs with multiple onsets on the injection of neutral beam, exploring the full spectral evolution using the fast digitizer is desirable. One such detailed description through the KSTAR shot 16 137 is described here. The shot discharge conditions are B_0 = 3.0 T, $I_p \sim 0.5$ MA, $\langle n_{e,\,\mathrm{int}}\rangle \sim 2.0 \times 10^{19}$ m^{-3} and the neutral beam is pulsed at 2 Hz with 10 ms beam ON time with 1.0 MW power. The filter-bank RF time traces along the with neutral beam power are shown in figure 4(a). The fast digitizer is triggered at 3.500 000 s, acquiring the RF emission signal continuously

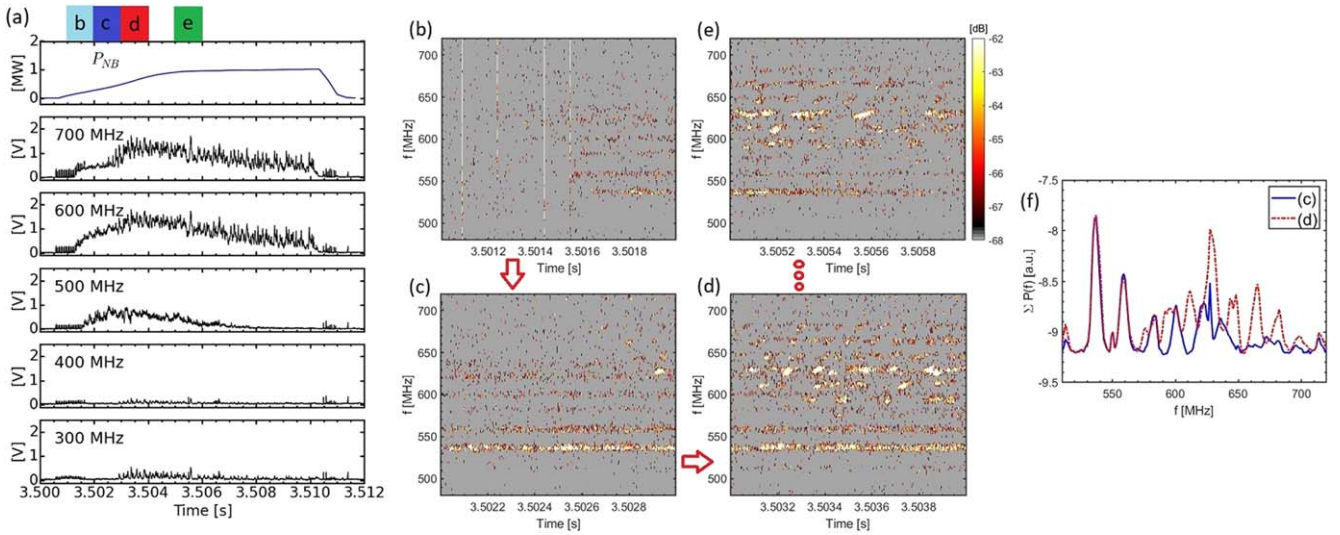

Figure 4. The full evolution of RF emission spectrum with neutral beam pulse through the filter-bank and fast digitizers for shot 16 137. Shot parameters: $B_0 = 3.0$ T, $I_p \sim 0.5$ MA and $n_{e,int} \sim 2.0 \times 10^{19}$ m^{-3}. (a) The time traces of filter-bank RF spectrometer along with neutral beam pulse. (b)–(d) Fully resolved RF emission spectra in 1 ms time windows illustrated by coloured blocks labeled according to the subfigure code, on top panel in figure 4(a), through the initial onset until saturation. (e) The emission spectrum as the intensity starts falling gradually as also depicted by green block in figure 4(a). The colour scale for spectrum plots in figures 4(b)–(d) is same as in figure 4(e). (f) The spectral power integrated over time for each frequency, on panels in figures 4(c)–(d) shows large peaks corresponding to high harmonics of deuteron cyclotron frequency.

through one pulse of the NBI period. The RF spectral evolution is obtained splitting the fast digitizer data in the time region of interest, into bins as described in section 2. The fully resolved RF emission spectra through the rise of RF emission and saturation phase are shown in figures 4(b)–(e). As the neutral beam power starts rising at 3.501 000 s, discrete and persistent emission lines, with frequency $\geqslant 540 \pm 1.2$ MHz, appear within 0.5 ms. The discrete emission lines appear with uniform line spacing of 21 MHz, corresponding to the deuteron cyclotron frequency at $R \sim 2.0$ m. Onset of the intense RF bursts occurs at ~3.503 000 s in the frequency range 595–665 $\pm$ 1.2 MHz. Even the RF bursts occur at discrete frequencies with successive line frequency spacing comparable to 21 MHz in some cases and deviations in other cases. A contrasting observation in this discharge is that the RF bursts occur at frequencies greater than the initial persistent emission line frequency as compared to that illustrated in figure 2(b). This observation in fast digitizer data is also consistent with the filter-bank RF signals depicted in figure 4(a). At a given frequency, for example the dominant frequency = 630 MHz, the time interval between the successive bursts is 100–200 μs. The persistent spectral lines in RF emission decrease in intensity gradually. On the other hand RF burst emissions appear with comparable intensity for ~10 ms, after which the beam is turned OFF.

The RF spectral evolution with the start of NBI suggests that more complex features exist in the spatio-temporal evolution of the fast ion distribution driving the instabilities. The rapid rise and saturation of RF emission indicates that wave excitation is saturated even with a small population of fast ions. The onset of RF bursts with a characteristic delay (1.5–2 ms) with respect to the initial RF emission onset give clues about further reorganization and radial spread to either side of the initial wave excitation region.

5. Other important factors possibly affecting the RF emission

5.1. Neutral beam OFF time before the next pulse injection

Since the RF emission exhibits rapid rise and gradual fall in intensity with characteristic timescales, the neutral beam OFF time might affect the RF emission on next pulse. Such a comparison is made between two KSTAR shots 19 116 and 19 336 as shown in figure 5. Summary of the discharge conditions for the shot 19 116 is $B_0 = 2.0$ T, $I_p \sim 0.6$ MA, $\langle n_{e,\,\mathrm{int}} \rangle \sim 2.7 \times 10^{19}$ m^{-3} and the neutral beam pulse is ON for 50 ms and OFF for 50 ms with a maximum power of 0.5 MW. The discharge conditions for the shot 19 336 are $B_0 = 1.8$ T, $I_p \sim 0.6$ MA and the neutral beam pulse is ON for 30 ms and OFF for 20 ms with a maximum power of 1.6 MW. Figure 5(a) illustrates the RF emission for the shot 19 116 through the filter-bank 600 MHz channel along with the neutral beam power. The RF emission intensity rise and decay trends are comparable with those of low duty cycle of neutral beam discussed in previous sections. The RF emission is onset soon with the neutral beam, at few persistent emission lines similar to that in figure 4(c), whereas the intense RF bursts onset with a delay of 1.5–2 ms similar to that in figure 4(d). The lower RF emission intensity may be due to significantly low neutral beam power used in this shot. For the shot 19 336 the RF emission is shown in figure 5(b) along with the neutral beam power. In this case the RF emission is delayed and purely bursty in nature as evident from the zero

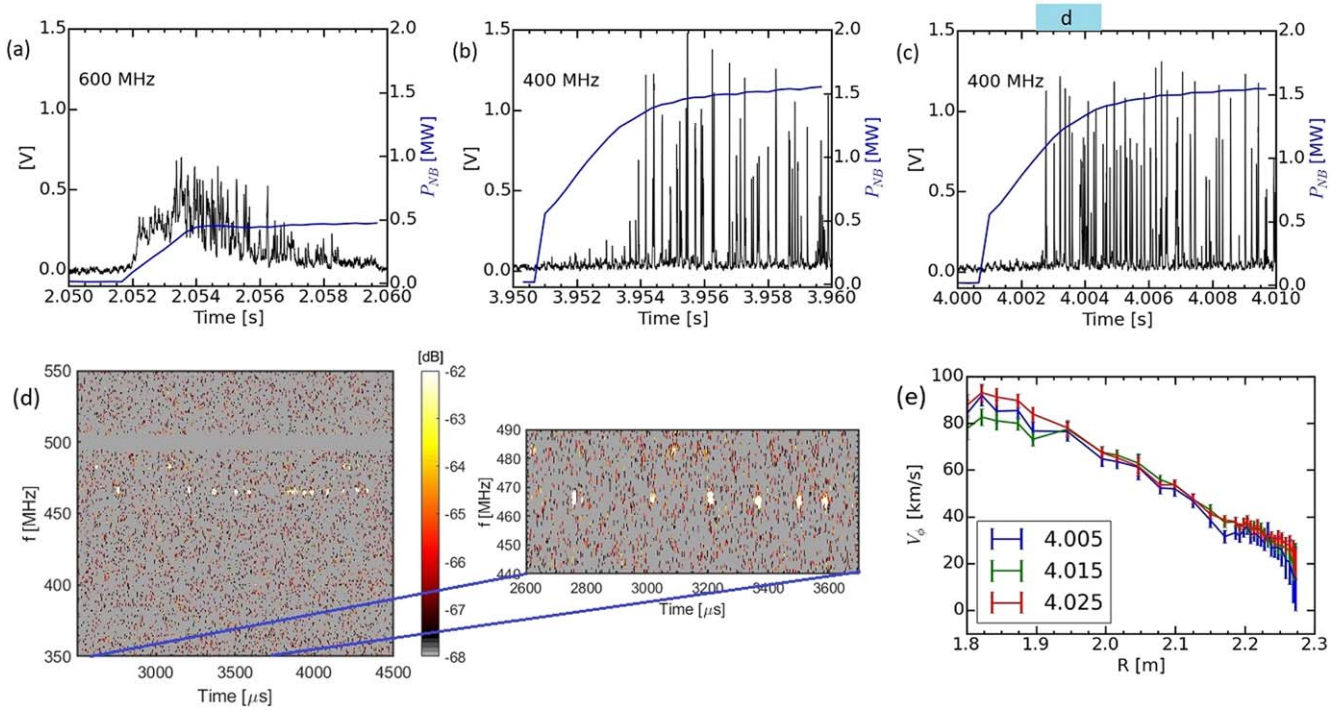

Figure 5. A comparison of RF emission for shots 19 116 and 19 336, each with different beam OFF time before injecting the next pulse. Shot parameters for 19 116: $B_0 = 2.0$ T, $I_p \sim 0.6$ MA, $\langle n_{e,\,\mathrm{int}} \rangle \sim 2.7 \times 10^{19}$ m^{-3}. Shot parameters for 19 336: $B_0 = 1.8$ T and $I_p \sim 0.6$ MA. (a) The filter-bank RF at 600 MHz and the neutral beam power (blue curve) time traces for 19 116 where the beam OFF time is 50 ms from the preceding neutral beam pulse. (b)–(c) The filter-bank RF at 400 MHz and the neutral beam power (blue curve) for 19 336 for two successive beam pulses where the beam OFF time is 20 ms from the preceding neutral beam pulse. (d) The RF emission spectrum from the fast digitizer for 19 336 in the time range depicted with cyan block labeled 'd' on top in figure 5(c). Intense RF bursts are confined mostly at 466 $\pm$ 1.2 MHz frequency which is within the bandwidth of the RF filter, that is 400 MHz $\pm$ 25%. The blow-up of (d) is shown on the right, which depicts first 6 RF bursts with decreasing time interval between consecutive bursts. (e) The toroidal rotation velocity at three instants during a neutral beam pulse starting at ~4 s for the shot 19 336. The major and minor radii are 1.8 m and 0.5 m respectively.

base line of the signal with spikes of ~20 μs duration each. The delay in the RF emission is possibly due to the lack of persistent emission lines, even though the RF bursts occur with high intensity. The disappearance of persistent emission lines, which would onset soon with neutral beam might be a consequence of decreasing the beam OFF time from 50 to 20 ms. The multiple onsets in the RF emission and evolution from persistent emission lines to bursty indicate possible redistribution or reorganization in the anisotropic distribution of fast ions. A characteristic timescale might exist within this limits (20–50 ms) after which the redistributed fast ion population decays to insignificant levels as the neutral beam is turned OFF. It is this timescale after which if the next beam pulse is injected, results in a fresh anisotropic fast ion distribution driving energetic ion driven modes with minimal effects from the preceding beam pulse.

There is another interesting observation evident from figure 5(b) with respect to the time interval of RF bursts. In the initial phase of RF emission onset (3.954–3.956 s) with the neutral beam, the time period between the bursts is nearly uniform and approximately 250 μs. This time period may be comparable to one toroidal transit time for the toroidal rotation velocity of 60 km s^{-1} at $R = 2.0$ m. This observation indicates possibly the RF burst source is toroidally localized. One more instance of RF emission from the shot 19 336 is shown in figure 5(c), for which the fast digitizer data for RF emission is also available. The corresponding spectral evolution is shown in figure 5(d) where zero (not shown) on the horizontal timescale would correspond to 4.000 000 s as included in figure 5(c). The RF burst emission is onset at 4.002 500 s, consistent with the filter-bank RF signal, predominantly at 466 $\pm$ 1.2 MHz except the few bursts appearing at 484 $\pm$ 1.2 MHz. The narrow emission frequency range indicates the RF burst source is radially localized too. The toroidal rotation velocity from the charge-exchange spectroscopy on KSTAR for the shot 19 336 during the neutral beam pulse starting at 4.0 s is shown in figure 5(e). The first instant of measurement for toroidal rotation velocity is available at 4.005 s and the velocity does not increase significantly further at the next instant. Therefore, the toroidal rotation velocity saturates in less than 5 ms on the NBI. The decreasing time interval from 250 to 90 μs for the 6 intense RF bursts at one unique frequency, lying between 4.002 760 and 4.003 590 s might indicate a steady increase in net toroidal rotation velocity for the perturbed structures containing the source of the RF burst emission. However, the toroidal rotation measurements with such high time resolution are currently not available and hence difficult to confirm at present.

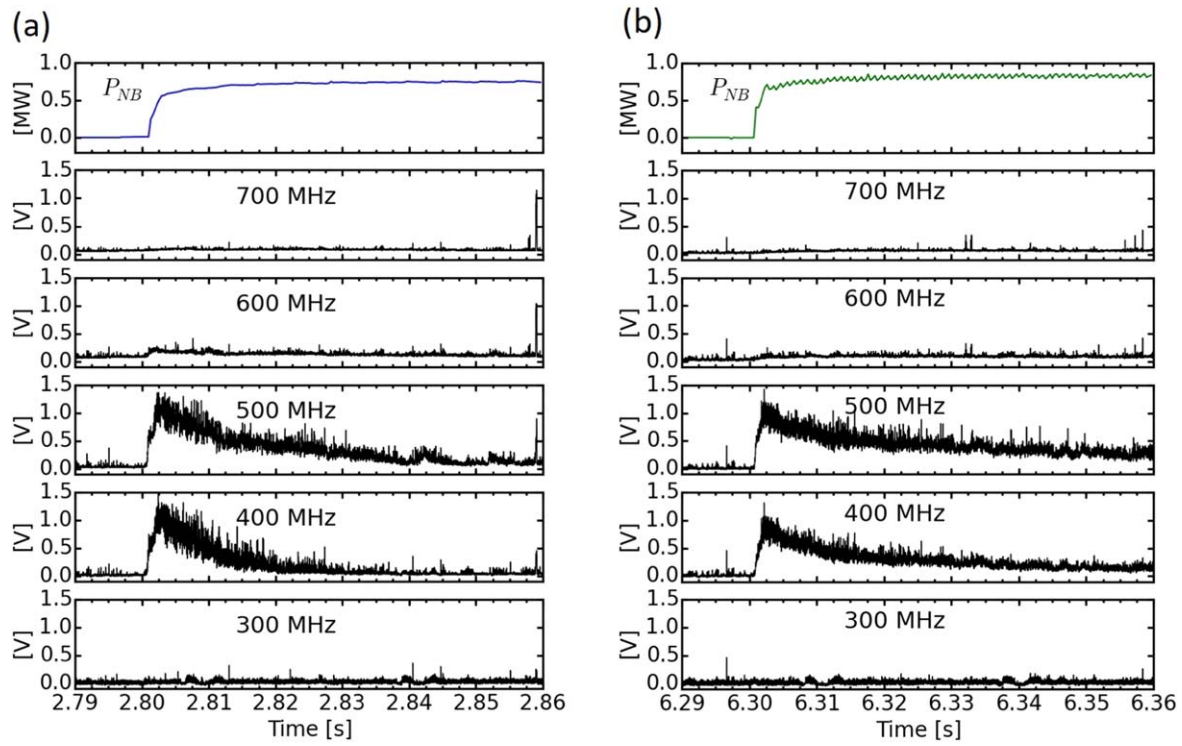

Figure 6. Comparison of the RF emission features with two neutral beamlines with different tangential radii for shot 17 010. Shot parameters: $B_0 = 2.2$ T, $I_p \sim 0.6$ MA, $\langle n_{e,\,\mathrm{int}} \rangle \sim 1.0 \times 10^{19}$ m^{-3}. (a) NB1A pulse ON at 2.8 s (b) NB1C pulse ON at 6.3 s. NB1C beamline has the least tangential radius. Comparable intensity of the RF emission, frequency range (400–500 MHz), rise and decay time are observed with the neutral beam injection at different angles.

5.2. Effect of the NBI angle

Two neutral beamlines of the KSTAR NBI system described in section 2 were used to inject pulses one from each beamline, at different time instants for the shot 17 010. The two beamlines labeled as NB1A and NB1C differ in the tangential radii of 1.486 m and 1.245 m from the major axis respectively and hence have the different injection angles. Summary of the discharge conditions for the shot 17 010 is $B_0 = 2.2$ T, $I_p \sim 0.6$ MA, $\langle n_{e,\,\mathrm{int}} \rangle \sim 1.0 \times 10^{19}$ m^{-3} and the neutral beam with a power of 0.8 MW and 0.2 s duration each, injected from NB1A at 2.8 s and from NB1C at 6.3 s. A lower beam energy of 60 keV for both NBI pulses was used in this discharge, compared to 70–100 keV for most of the results described in previous sections. Electron cyclotron heating power of 0.8 MW was also applied prior to each neutral beam pulse. The time traces of RF emission through the filter-bank RF spectrometer along with the neutral beam pulse are shown in figure 6. The RF emission spectrum (400–500 MHz) and the intensity appear comparable for the two beam pulses. The rise time (∼2 ms) and decay time (∼20 ms) in intensity are also found comparable for the two beam pulses. These observations imply that the time evolution of anisotropic fast ion population and the frequency range of the induced instabilities are approximately similar for both angles of NBI. The rapid rise followed by gradual decay over 20 ms indicate the typical time scale of population inversion on the LFS with the NBI, which is much shorter than the electron slowing down time (∼100 ms). More detailed comparisons and contrast in the RF spectral evolution will be attempted from the fast digitizer acquisition in future works.

6. Mechanism driving the waves in RF emission frequency range

The RF emission on neutral beam injection and its spectral features described in previous sections indicate the emission occurs in discrete spectral lines. The observed spectral lines correspond to the high harmonics of deuteron cyclotron frequency at $R \sim 2.0$ m and overlap with the range of f_{LH} over a broad region on LFS. These observations indicate that the fast ions originating from the neutral beam are primarily responsible for the wave excitation in RF emission frequency range. The LH instability due to 'double resonance' condition between f_{LH} and high harmonics of beam ion cyclotron frequency proposed by Suvorov *et al* seems a plausible mechanism [13]. This instability mechanism was proposed to explain the LH turbulence observed in W7-AS with perpendicular injection of weak diagnostic neutral beam, but not observed with the heating neutral beams. A low thermal ion temperature (<0.6–0.8 keV) required as a threshold criteria for this instability and the constant magnitude of turbulent fluctuation amplitude with the neutral beam (∼50 ms) on W7-AS appear in contrast with the results reported in this article. The applicability of this instability for the wave excitation in RF emission frequency range, therefore, needs further investigation.

The rapid saturation (~2 ms) in RF emission intensity followed by gradual decay (~20 ms) reported here motivate for exploring an alternate plausible mechanism. Since the neutral beam deposition is efficient deep in the core ($R \leqslant$ 1.8 m) initially, only a small population of fast ions is produced along the beam path in the region midway between the magnetic axis and the edge (1.9 m $< R <$ 2.1 m). The numerical analysis for the neutral beam deposition in KSTAR indicates large pitch angle is possible for the fast ions originating on the low field side [12]. A fraction of this initial small population of fast ions possesses large gyro-radius with perpendicular velocity exceeding the ion acoustic velocity. Since the wavelengths for LH frequency range can be comparable or smaller than the fast ion gyro-radius, the fast ions can appear as drifting across the field, satisfying the criteria for the excitation of lower hybrid drift instability (LHDI) [14]. The excitation of LHDI due to cross-field current arising from large fast ion gyro-radius was observed near the magnetic axis of the tokamak or magnetic island in TEXTOR tokamak [15, 16]. Generation of effective cross-field current arising from small population of fast ion on LFS in the initial phase of neutral beam injection and the excitation of LHDI for results reported here, needs further investigation. Increase in fast ion population on LFS can result in random gyro-orbits through each small volume, resulting in a negligible cross-field current, hence damping of the excitation source of these waves. In previous works, using the particle-in-cell (PIC) simulations, the drifting minority population of the fusion products in tokamaks were found to excite waves in f_{LH} range, predominantly electrostatic in nature [17, 18].

A favorable scenario for the occurrence of fast waves at ion cyclotron harmonics can be understood as follows, if the fast ions are assumed like a minority population. The obliquely propagating (nearly perpendicular) waves will encounter two different resonant locations for the ion cyclotron frequency, one each with the thermal ions and the fast ions. If the finite parallel wavenumber is parallel to the fast ion parallel velocity (hence co-propagating), the ion cyclotron resonance layer for the fast ions occurs at a further interior radial location due to Doppler shift, compared to the resonance layer for thermal ions. Hence an ion-ion hybrid layer should occur between the two ion cyclotron resonant layers. It is well known that a fast wave launched from the antennas outside the plasma gets mode-converted to ion Bernstein waves or cold ion cyclotron waves at this hybrid layer [19, 20]. For the observations in the present context, a reverse process to the above mode conversion is a plausible mechanism [21]. However, the resonance with local f_{LH} seems an important criterion [22], as the RF emission is at discrete lines, mostly the ion cyclotron harmonics overlapping with the f_{LH} range on the LFS. Hence, a favorable condition for wave excitation in the lower hybrid frequency range at ion cyclotron harmonics is possible for a small population of fast ions from the neutral beams. Identification of these plasma waves at ion cyclotron harmonics and coupling with instabilities in f_{LH} range may be attempted using PIC simulations in near future.

In another recent work using the PIC simulations, assuming a narrow range of pitch angle for fast ions (80°–84°) from the neutral beam resulted in particle orbits through the edge region of the KSTAR [23]. This non-Maxwellian distribution of fast ions is found capable of driving magnetoacoustic cyclotron instability, and potentially explains the RF emission at the harmonics of deuteron cyclotron frequency at the edge in KSTAR high confinement mode plasma [8, 9]. The localized non-Maxwellian fast ion distributions in a broad region on LFS, resonantly exciting the instabilities at deuteron cyclotron harmonics in f_{LH} range is another possible source of RF emission in low confinement mode plasmas reported here.

7. Summary

Extensive observations on electromagnetic emissions with the tangential neutral beam injection in KSTAR L-mode plasma and plausible mechanisms causing the emission are reported here. Multiple onsets in the RF emission and characteristic evolution in the emission spectrum are found with the beam injection. The initial RF emission onset occurs persistently at discrete frequencies, starting soon with the neutral beam injection (<1 ms). The discrete frequencies correspond to the high harmonics of deuteron cyclotron frequency at a location midway between the magnetic axis and the edge. As the RF emission intensity becomes saturated, intense RF bursts onset broadening the frequency range further, on either high or low frequency side. The intense RF bursts also occur at discrete frequencies, however, deviations in the frequency spacing through successive bursts are observed in some cases. The RF burst emission in some cases, with narrow spectral character and repetition frequency comparable with the toroidal rotation frequency, within the available time resolution, hint at possible spatial localization of the RF emission source. More accurate comparisons can be useful in predicting the spatio-temporal evolution of anisotropic distribution of fast ions in detail. The observed spectral lines mostly overlap with the lower hybrid frequency range in a broad region on the LFS indicating the excitation of instabilities in lower hybrid frequency range driven by the cross-field fast ion drift or the double resonance with ion cyclotron harmonics. The discrete nature of the RF emission spectrum, with spacing comparable to the deuteron cyclotron frequency, at local lower hybrid frequencies suggests a possible resonance mechanism with the ion cyclotron emission mechanism. The present observations provide a novel insight for the interpretation of the neutral beam deposition in a tokamak and the energetic particle driven instabilities.

Acknowledgments

This work is supported by National Research Foundation of Korea under contract No. NRF-2019M1A7A1A03088456 and BK21 + program.

ORCID iDs

Shekar G Thatipamula https://orcid.org/0000-0003-2816-5862
M H Kim https://orcid.org/0000-0002-7481-4600
J H Kim https://orcid.org/0000-0001-7792-3581
G S Yun https://orcid.org/0000-0002-1880-5865

References

[1] Gorelenkov N N, Pinches S D and Toi K 2014 *Nucl. Fusion* **54** 125001
[2] Reiter D, Wolf G H and Kever H 1990 *Nucl. Fusion* **30** 2141
[3] Dendy R O, Lashmore-Davies C N, McClements K G and Cottrell G A 1994 *Phys. Plasmas* **1** 1918
[4] Gorelenkov N N and Cheng C Z 1995 *Nucl. Fusion* **35** 1743
[5] Heidbrink W W 2008 *Phys. Plasmas* **15** 055501
[6] Crocker N A *et al* 2013 *Nucl. Fusion* **53** 043017
[7] Leem J, Yun G S and Park H K 2012 *J. Instrum.* **7** C01042
[8] Thatipamula S G *et al* 2016 *Plasma Phys. Control. Fusion* **58** 065003
[9] Kim M H *et al* 2018 *Nucl. Fusion* **58** 096034
[10] Chapman B *et al* 2017 *Nucl. Fusion* **57** 124004
[11] Chapman B *et al* 2018 *Nucl. Fusion* **58** 096027
[12] Kim J Y *et al* 2016 *AIP Adv.* **6** 105013
[13] Suvorov E V *et al* 1998 *Nucl. Fusion* **38** 661
[14] Krall N A and Liewer P C 1971 *Phys. Rev.* A **4** 2094
[15] Nielsen S K *et al* 2013 *Plasma Phys. Control. Fusion* **55** 115003
[16] Marchenko V S and Reznik S M 2015 *Plasma Phys. Control. Fusion* **57** 045006
[17] Cook J W S, Chapman S C, Dendy R O and Brady C S 2011 *Plasma Phys. Control. Fusion* **53** 065006
[18] Cook J W S, Dendy R O and Chapman S C 2011 *Plasma Phys. Control. Fusion* **53** 074019
[19] Brambilla M and Ottaviani M 1985 *Plasma Phys. Control. Fusion* **27** 1
[20] Nelson-Melby E *et al* 2003 *Phys. Rev. Lett.* **90** 155004
[21] Ji H, Kulsrud R, Fox W and Yamada M 2005 *J. Geophys. Res.* **110** A08212
[22] Toida M *et al* 2019 *Plasma Fusion Res.* **14** 3401112
[23] Chapman B *et al* 2019 *Nucl. Fusion* **59** 106021